Surfactant Removal and Silica Condensation during the Photochemical Calcination of Thin Film Silica Mesophases

Andrew M. Dattelbaum,*,† Meri L. Amweg,†,‡ Julia D. Ruiz,† Laurel E. Ecke,† Andrew P. Shreve,† and Atul N. Parikh‡

Bioscience Division, Los Alamos National Laboratory, Los Alamos, New Mexico 87545, and Department of Applied Science, University of California, Davis, California 95616

Received: March 17, 2005; In Final Form: May 31, 2005

The evolution of photochemical surfactant removal and silica condensation from organically templated thin film silica nanocomposites with mesoscopic ordering has been probed using a combined application of Fourier transform infrared (FT-IR) spectroscopy and single wavelength ellipsometry. Thin films of silica nanocomposites were prepared by a previously reported evaporation-induced self-assembly process. Specifically, oxidized silicon and gold substrates were withdrawn at 25 mm/min from a subcritical micelle concentration solution containing an ethylene oxide surfactant as a structure-directing agent and tetraethyl orthosilicate as a silica precursor. Real-time grazing incidence difference FT-IR spectra of the nanocomposite films on gold taken during exposure to short-wavelength ultraviolet light (184−257 nm) show that surfactant removal and silica condensation occur gradually and concomitantly. Surfactant removal and silica reconstructions were found to be nearly complete after 90 min of exposure. Further, a transient feature was observed in the FT-IR spectra around 1713 cm^{-1} during the UV exposure process and was assigned to a carbonyl (C═O) stretching mode absorption, reflecting the transient formation of a partially oxidized surfactant intermediate. From these data we propose a stepwise model for surfactant removal from the nanocomposite films. Ellipsometrically determined index of refraction values collected as a function of UV exposure are also shown to support such a stepwise mechanism of surfactant removal from the ordered nanocomposite silica thin film mesophases studied here.

Introduction

Nanostructured, mesoporous materials, both bulk[1] and thin films,[2−4] have attracted considerable attention in recent years due to their usefulness in catalysis, their usefulness in separations,[5−9] and their many emerging applications as structured hosts in the design of new functional materials, including electronic and photonic materials.[10−17] Such materials are typically formed using a self-assembled, ordered organic phase that templates the formation and growth of the inorganic silica in templated sol−gel synthesis processes.[18] For many applications, the usefulness of these materials relies on the ability to remove the organic surfactant phase while maintaining the porous structure of the resultant inorganic framework. High-temperature calcination (∼450 °C) is the most commonly employed procedure for template removal and has been systematically studied by several groups.[19−22] However, high-temperature calcination is not suitable for surfactant removal from ordered nanocomposite films deposited on temperature-sensitive surfaces, such as thin metal films, or for the selective removal of surfactant from specific regions of an ordered nanocomposite film.

To overcome the limitations of thermal calcination, several nonthermal surfactant removal techniques to make mesoporous thin films, such as solvent extraction,[23] are being explored. More recently, we and others have developed a photochemical alternative following simple UV or UV/ozone treatments.[24−26] These UV-based photochemical treatments are particularly attractive as they have been used extensively by the semiconductor industry to break down small amounts of organic impurities on surfaces into low vapor pressure molecules, such as CO_2 and H_2O.[27] Our process uses inexpensive and readily available equipment at near-ambient temperatures and is suitable for patterned surfactant removal[28] or for surfactant removal from films deposited on temperature-intolerant substrates. However, the mechanism by which the surfactant is removed and silica is condensed during the calcination has not been established. A systematic study aimed at understanding the mechanism of UV photocalcination and determining the cooperativity of the surfactant removal and silica condensation processes will provide significant insight to help optimize the method's application, establish its generality, and develop a lateral and thickness control over the calcination process useful for generating two- and three-dimensionally patterned thin-film silica mesophases.

Here, we report an investigation of how short-wavelength UV light interacts with ordered nanocomposite silica thin films to remove the organic templating phase and condense silica using a real-time application of Fourier transfrom infrared (FT-IR) spectroscopy and ellipsometry. Our results confirm a continuous and gradual removal of the surfactant phase via oxidation with an attendant condensation of the silica framework. The silica condensation occurs in a process remarkably parallel to the surfactant removal process. Our results also suggest a simple stepwise kinetic model for the surfactant removal where oxidized surfactant intermediates form before the organic material is ultimately lost to the surroundings in the form of low vapor pressure molecules.

† Los Alamos National Laboratory.
‡ University of California.

10.1021/jp051401+ CCC: $30.25
Published on Web 07/13/2005

Experimental Section

Surfactant/silicate thin films were prepared following a previously described two-step process that was designed to minimize silicate condensation and promote facile silica/surfactant self-assembly during film deposition.[29] Initially, a silica sol was prepared by refluxing a mixture of tetraethyl orthosilicate (TEOS; Aldrich, 61 mL), anhydrous ethanol (Fisher, 61 mL), ~18 MΩ deionized water (0.44 mL), and 0.07 N hydrochloric acid (HCl, 0.2 mL) at 60 °C. Upon cooling to room temperature, a part of the above solution was diluted with ethanol, water, and hydrochloric acid (0.07 N). A nonionic surfactant, $C_{16}H_{33}(OCH_2CH_2)_nOH$, where $n \sim 10$ (technical name Brij56, Aldrich), was then added to the silica sol solution at ~4.0 wt %, significantly below the critical micelle concentration (cmc). During the addition of the surfactant, the water, ethanol, and hydrochloric acid concentrations were adjusted to yield the final reactant mixture in the mole ratios of 1 TEOS: 22 C_2H_5OH:4 H_2O:0.004 HCl:0.085 Brij56. Mesostructured silica thin films (also referred to as ordered nanocomposites in this paper) were deposited by withdrawing the substrate from the 4 wt % Brij56/TEOS solution at 2.5 cm/min. Freshly oxidized single-crystal silicon (100) with a native oxide overlayer (SiO_2/Si) was used as the substrate for ellipsometry measurements, while a freshly evaporated Au metal film (2000 Å), supported on piranha-cleaned glass with a 50 Å Ti primer as an adhesion promoter, was used for grazing incidence FT-IR spectroscopy measurements. The mesostructures of the substrate-supported nanocomposite silica thin films derived in this manner were verified using X-ray diffraction (XRD) recorded on a Siemens XDS200 diffractometer using a Peltier detector that eliminates white radiation and beta lines with $\lambda = 1.5418$ Å in $\theta-2\theta$ ($2\theta = 1-6°$) scan mode using a step size of 0.02°/min.

UV-induced photocalcination was achieved by exposing ordered nanocomposite silica thin films to UV light generated from a low pressure Hg lamp (pen or grid lamps purchased from Ultraviolet Products, Inc.). Exposure times required for surfactant removal can vary with age and intensity of the UV source, as well as with the spatial proximity of the source to the sample. Those presented here are typical for relatively new grid lamp sources placed approximately 2 cm above the substrate. The resulting mesoporous silica thin films exhibited cubic ordering as determined by XRD measurements (data not shown), which is consistent with our previously reported work.[26]

FT-IR spectra were obtained in grazing incidence, specular-reflection mode at an 80° angle of incidence. Spectra were collected using a nitrogen-purged Bruker Equinox 55 Fourier transform infrared spectrophotometer and a DLA-TGS detector. All reported spectra were obtained by co-adding multiple scans collected at 4 cm^{-1} resolution. Reference samples used were the gold films freshly evaporated immediately prior to mesostructured film deposition. Integration of the area under selected bands in the FT-IR data was accomplished using the integration option in Grams v3.2. For data where overlapping bands were observed the bands were decomposed into two or three peaks using a mixed Gaussian/Lorentzian model prior to integration.

Single wavelength ellipsometry measurements were taken with a nulling ellipsometer (Rudolph Research, Piscataway, NJ) operating at 632.8 nm and 70° angle of incidence. Ellipsometric values of Δ and Ψ were collected for the ordered nanocomposite silica thin films on both silicon and freshly evaporated gold on glass substrates as a function of UV exposure. The indices of refraction of the cleaned substrates were determined ellipsometrically prior to thin film deposition. All the index of refraction (n) and thickness data for nanocomposite films were calculated from the Δ and Ψ values following a classical electromagnetic theory of layered media using an ambient−film−substrate model.[30]

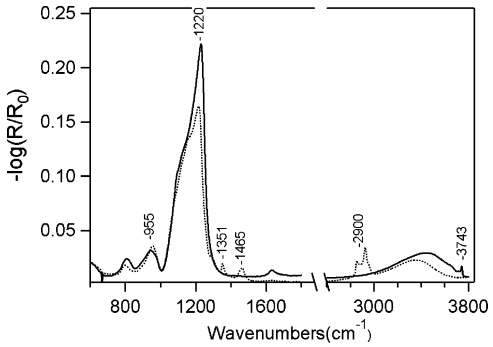

Figure 1. Grazing incidence FT-IR spectra (80° incidence) of Brij56 templated nanocomposite silica film before (dotted line) and after (solid line) exposure to deep-UV light for 180 min.

Results and Discussion

Grazing Incidence FT-IR Spectroscopy. Grazing incidence FT-IR spectra of an ordered nanocomposite silica thin film on a gold substrate before and after exposure to deep-UV light (185−254 nm) for 3 h are shown in Figure 1. The spectrum of the as-prepared samples (before UV exposure) reveal a number of characteristic features confirming the presence and integrity of the surfactant and silicate phases of the as-prepared templated silica thin film on gold. The set of overlapping peaks due to methylene ($-CH_2$) and methyl ($-CH_3$) C−H stretching vibrations from the alkyl tails of the Brij surfactant[31] is prominent in the region between 2700 and 3100 cm^{-1}. The two discernible maxima at 2854 and 2923 cm^{-1} can be straightforwardly assigned to the methylene symmetric and antisymmetric vibrations, respectively, whereas the methyl symmetric and asymmetric bands at 2878 and 2956 cm^{-1} can be identified in the second derivative analyses (not shown) of the observed spectra. The presence of weaker, but reproducible, C−H rocking modes at 1465 and 1351 cm^{-1} further confirms the surfactant phase in the mesophase.[32,33] The silica phase is characterized by four regions of the spectra. First, the presence of an intense band between 1000 and 1300 cm^{-1} is due to the silicate (Si−O) antisymmetric stretch.[32−35,38] Second, a broad band centered at 955 cm^{-1} due to the Si−O stretching modes of silanol (Si−OH) groups[34−36] confirms unpolymerized silanols in the film. Third, the band centered around 800 cm^{-1} is due to the symmetrical Si−O stretch.[32−35,37] Fourth, a broad envelope spanning ~3000−3600 cm^{-1} is observed. This feature can be straightforwardly assigned to the hydrogen bonded silanol groups with absorbed molecular water at the film surface. The feature also incorporates vibrational bands due to silanols and water present at the internal defect sites (see below).[36,37] These spectral characteristics are in excellent agreement with those reported previously for as-prepared mesostructured silica thin films.[26]

After exposure of the ordered nanocomposite silica film to deep-UV light for an extended period (~3 h) (solid trace in Figure 1), several noticeable changes in the IR spectrum occur. All of the peaks assigned to the C−H stretching modes of the surfactant microphase (2700−3100 and 1450−1350 cm^{-1}) vanish below the noise level (1×10^{-4} au) in the spectrum, which is consistent with the nearly complete removal of the Brij56 surfactant from the film. The broad envelope from 3000 to 3600 cm^{-1} shifts to higher energy, and a distinct, sharp feature

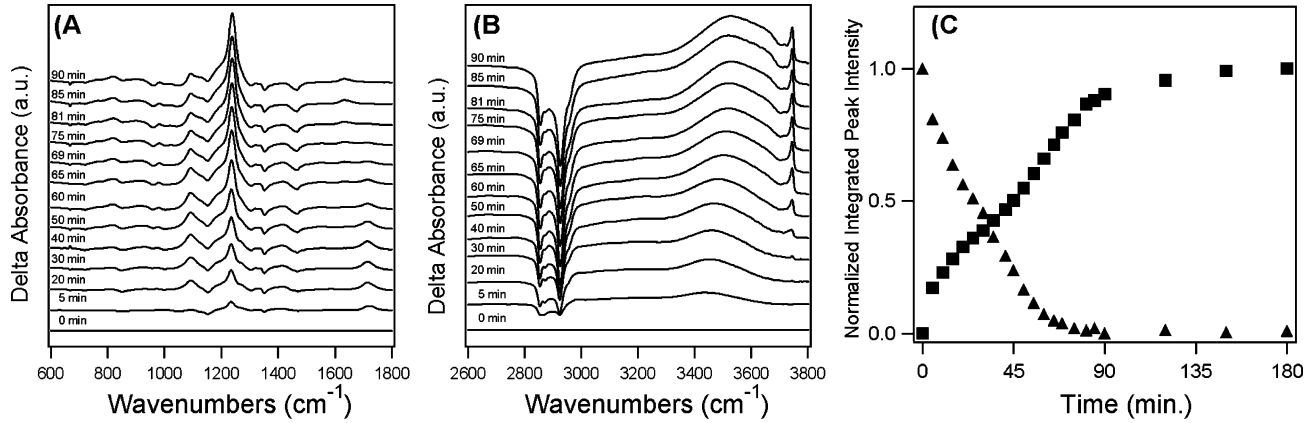

Figure 2. Grazing incidence FT-IR difference spectra (80° incidence) for Brij56 templated nanocomposite silica thin film dip-coated on a freshly evaporated Au surface as a function of deep-UV exposure between (A) 600−1800 and (B) 2600−3800 cm^{-1}. The as-prepared surfactant/silicate thin film is used as the baseline at $t = 0$ min. (C) Normalized integrated peak intensity for Si−O stretching modes (■, 1305−1153 cm^{-1}) and C−H modes (▲, 3010−2680 cm^{-1}) shown in panels A and B.

appears at 3743 cm^{-1}, which is assigned to the free silanol (Si−OH) stretching mode.[35,37,38] The shift of this envelope indicates a change in the hydrogen bonding interactions within the film, which is consistent with the partial uptake of water into the mesoporous silica. However, complete filling of the pores would also have resulted in removal of the free silanol mode from the FT-IR spectra. A rise in the integrated intensities for the Si−O−Si antisymmetric stretching mode absorptions (a broad envelope in the 1000−1300 cm^{-1} region) further confirms that deep-UV treatment promotes silanol condensation to form additional Si−O−Si bonds upon surfactant removal from the nanocomposite silica thin film. These changes are entirely consistent with those reported by us in a previous study.[26]

Grazing angle FT-IR difference spectra were collected in real time as a function of UV exposure time to monitor the surfactant removal and silica reconstruction processes. Selected regions of the FT-IR data taken as a function of UV exposure from $t =$ 0 min to $t =$ 90 min are shown in Figures 2 and 3 as the difference spectra from the initial mesostructured silica thin film. The traces shown in Figures 2 and 3 report on cumulative spectral changes as a function of total exposure period. Thus, at time $t = 0$ the spectrum appears flat (bottom trace). At later times, bands observed in the difference spectra reveal changes relative to the initial mesostructured phase. Bands that grow in the negative direction indicate features that are removed from the initial nanocomposite film spectrum, while bands that gain intensity in the positive direction indicate either an increase in intensity for features already present in the nanocomposite film spectrum or the emergence of new vibrational spectral features arising from newly formed species.

The results in Figure 2 show the gradual and continuous loss of intensity for the vibrational modes between 2700 and 3100 cm^{-1} assigned to the C−H stretching modes of the surfactant. Concomitant decreases are also observed in the intensity of modes at 1457 and 1351 cm^{-1} assigned to C−H bending modes of the surfactant. Changes in the broad envelope found between 2700 and 3500 cm^{-1} indicate water restructuring upon surfactant removal. In this same region, terminal hydroxy groups, Si−OH (3744 cm^{-1}), are observed to form after approximately 20 min of UV exposure. As shown in Figure 2A, there is also a gradual intensification of the vibrational mode at 1196 cm^{-1}, the Si−O−Si asymmetric stretch, with increasing time of UV exposure.

Changes in the infrared spectrum of the surfactant templated silica thin film as a function of UV exposure time are clearly shown by integrating the area of the prominent features in the

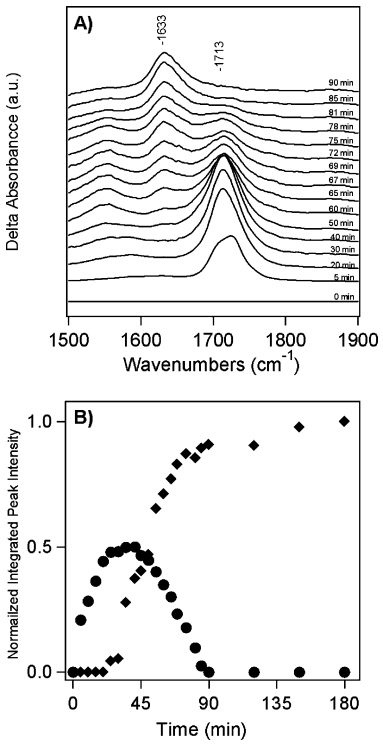

Figure 3. (A) Grazing incidence FT-IR difference spectra (80° incidence) for Brij56 templated nanocomposite silica thin film dip-coated on a freshly evaporated Au surface as a function of UV exposure (0−90 min) in the region between 1500 and 1900 cm^{-1}. (B) Normalized integrated peak intensity for the bands at 1633 (◆) and 1713 cm^{-1} (●) shown in (A).

FT-IR difference spectra (Figure 2C). Integrated intensities for the antisymmetric Si−O modes (1305−1153 cm^{-1}) and the C−H stretching modes (3010−2680 cm^{-1}) show the increasing and decreasing intensity of the C−H and Si−O modes, respectively, as a function of UV exposure time.

The difference spectra in the region between 1500 and 1900 cm^{-1} are shown on an expanded scale in Figure 3A. This spectral region is initially dominated by a transient mode at 1713 cm^{-1}, which increases with UV exposure time up to 40 min, and then gradually disappears from the spectrum upon longer UV exposure times. As this band at 1713 cm^{-1} decreases in intensity, a band at 1633 cm^{-1} gains intensity and remains strong at the end of the UV treatment. Integrated intensities for the

vibrational modes centered at 1633 and 1713 cm^{-1} are shown in Figure 3B.

The data presented above show that the surfactant removal and silicate reconstruction processes occur gradually and concomitantly with increasing UV exposure. After approximately 90 min of deep-UV exposure, the bands associated with the C−H stretching modes of the surfactant are no longer observed in the IR spectra, and no further evolution is observed in the difference spectra in the corresponding spectral region (see Figure 2C). Further, surface area measurements previously reported by us established that loss of the C−H modes in the FT-IR spectra indicated the formation of a highly porous and ordered silica thin film after 120 min of deep-UV exposure.[26] These data demonstrate that, under these experimental conditions, ∼90 min is required for nearly complete surfactant removal using deep-UV light, which may be compared to the 4−6 h process for thermal calcination or solvent extraction of the surfactant template.[39] However, additional small increases in the integrated intensity of the silica modes between 1305 and 1153 cm^{-1} are observed from 90 to 180 min of UV exposure (Figure 2C), suggesting that Si−O condensation continues to occur to some extent after the surfactant has been removed from the film.

The spectral features between 1500 and 1900 cm^{-1} shown in Figure 3 provide powerful diagnostic markers in assessing the chemical transformations of the surfactants during the photochemical calcination process. In this regard, detailed analyses of these spectral changes can be used to conclusively assess the mechanism by which surfactant removal from these thin films occurs. The band centered at 1633 cm^{-1} can be assigned to the water-bending mode commonly found in this region.[25] This assignment was confirmed by immersing films exposed to UV light for 60 min in deuterium oxide (D_2O), which resulted in a shift to lower energy for the mode at 1633 cm^{-1}, as expected upon proton−deuteron exchange (see Supporting Information). By contrast, the transient band at 1713 cm^{-1} was unaffected upon exposure to D_2O. Devlin et al. have previously observed that peaks in the 1700 cm^{-1} region can be due to confined water clusters.[40] However, our deuteration experiment establishes that the peak at 1713 cm^{-1} observed for the ordered nanocomposite silica thin films does not originate from such clusters within the pore channels. The band at 1713 cm^{-1} is, however, consistent with a carbonyl (C═O) mode absorption in a nanocomposite silica thin film.[32,41] The presence of such carbonyl modes can be explained by recognizing that deep-UV light (185−254 nm) generates oxygen radicals and ozone that can oxidize the surfactant material.[42] Similar bands in this region have been observed during the UV/ozone exposure of silicon−carbon polymers and were also assigned to carbonyl-containing intermediates.[43,44] Therefore, we similarly conclude that the highly reactive oxygen species generated by deep-UV light react with the surfactant to generate partially oxidized intermediates that initially accumulate within the nanocomposite film, which leads to the increases observed in the mode centered at 1713 cm^{-1}. With increased UV exposure times these intermediates are oxidized further to small volatile molecules, such as CO_2 and H_2O, which can readily escape from the thin film, as indicated by the diminishing intensity for the absorption at 1713 cm^{-1}. The band at 1713 cm^{-1} is thus a direct marker of oxidized surfactant intermediates formed during UV light exposure.

To further support the role of ambient oxygen in surfactant removal, ordered nanocomposite films were also exposed to deep-UV light under reduced oxygen atmospheres (nitrogen-purged box with a relative humidity <3%). After 90 min of deep-UV exposure ∼35% of the initial surfactant was still present in the films (see Supporting Information), and complete surfactant removal occurred only after an additional hour of the UV treatment. We note that although these latter experiments were performed in a nitrogen-purged environment, there is still likely molecular oxygen absorbed in the thin film itself, and reactive oxygen species may also be produced during the photodegradation of the oxygen-containing organic surfactants.

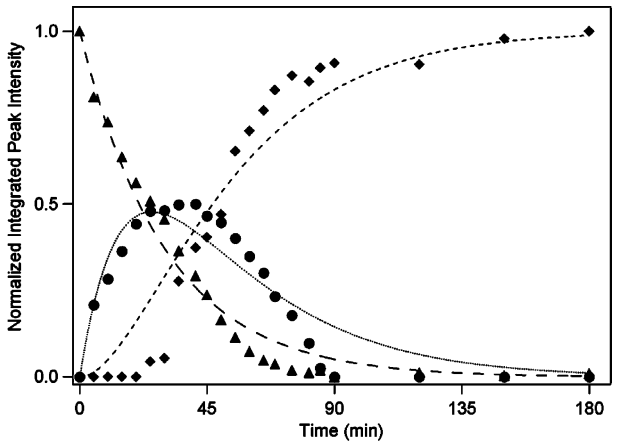

Figure 4. Plot of normalized integrated peak intensity for C−H modes (▲, 3010−2680 cm^{-1}) shown in Figure 2B, as well as transient carbonyl mode at 1713 cm^{-1} (●) and water bending mode at 1633 cm^{-1} (◆). The dashed lines are fits of the data from a simple sequential kinetic model (see text).

The results presented in this study confirm that the exposure to short-wavelength UV radiation leads to a continuous and gradual removal of surfactants while simultaneously strengthening the silicate framework. This is remarkably similar to the thermal calcination process. Real-time application of the infrared data can be reconciled into a single mechanistic scenario where the surfactant oxidation allows an effective two-step photooxidation pathway. We can then summarize surfactant removal from the nanocomposite films by eq 1:

$$\text{surfactant} \xrightarrow{k_1} (C(O))_x \xrightarrow{k_2} H_2O + CO_2 \qquad (1)$$

In eq 1, $(C(O))_x$ represents the entire family of partially oxidized, carbonyl-containing, compounds that may be produced from the surfactant. Using this simple model, approximate fits to the integrated intensity data obtained by the grazing incidence FT-IR measurement may be found, as shown in Figure 4. Normalized integrated intensities of the surfactant C−H modes were used to represent the initial starting phase, the carbonyl mode at 1713 cm^{-1} was used to approximate the intermediate phase, and the water-bending mode at 1633 cm^{-1} was used to represent the final product phase. This simple analysis strongly supports the overall sequential nature of the oxidative removal of the surfactant from the films during the deep-UV photocalcination process.

Ellipsometric Data. Index of refraction data for an ordered nanocomposite silica thin film determined as a function of UV exposure are shown in Figure 5 (see Supporting Information for a table of actual values with estimated errors). In this case the sample was monitored periodically for a total of 170 min of UV exposure. An initial value of ∼1.46 was calculated for the surfactant templated nanocomposite film, which is consistent with values reported elsewhere.[45] Index of refraction changes during the initial UV exposure (5−10 min) were observed to be minimal. However, after this initial exposure time, with

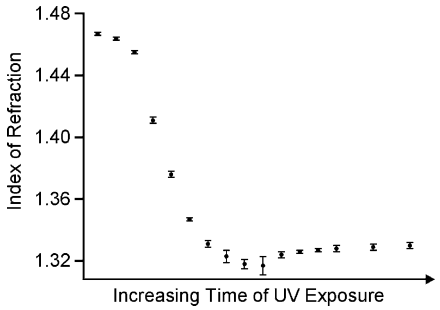

Figure 5. Ellipsometrically determined index of refraction for ordered Brij56 templated nanocomposite silica thin film as a function of deep-UV light exposure.

subsequent UV exposure, the index rapidly drops to a value of 1.32 before rising slightly during the final UV exposure times.

These index of refraction data also support a stepwise mechanism for surfactant removal. The ordered nanocomposite thin film can be thought to be comprised of one-third sol−gel silica ($n \sim 1.49$) and two-thirds organic phase ($n \sim 1.45$) distributed evenly throughout the film, which results in the observed value of 1.46 for the as-prepared film. As seen in Figure 5, index of refraction changes from the initial UV exposure (5−10 min) are minimal as the surfactant is partially converted to an oxidized form, but remains within the film with approximately the same index of refraction. With increasing UV exposure, and subsequent oxidation reactions, the surfactant oxidation products begin to escape from the film, resulting in partially empty void space ($n_{air} = 1.0$) within the pores. That this is the case is indicated by our observation that the index of refraction for the porous film even falls slightly below the index of refraction for water ($n_{water} = 1.33$, $n_{film} = 1.32$) at its lowest value. Upon reaching this minimum value the index of refraction begins to slowly rise upon further UV exposure, which can be explained by partial filling of the pores with water. After complete surfactant removal and with no further UV exposure, the index of refraction continues to rise over the next 24−48 h after complete surfactant removal and ultimately flattening out at ∼1.4 (data not shown), indicating nearly complete filling of the pores with water due to capillary action. For this latter process, similar index of refraction results determined by spectroscopic ellipsometry have been previously reported by Brunet-Bruneau et al.[46] and were consistent with the gradual uptake of water by the mesoporous film from the environment. These data are also consistent with the infrared spectra collected as a function of UV exposure time, which showed the water-bending mode at 1633 cm^{-1} to become more intense with increasing UV exposure. Further, the free silanol mode, 3743 cm^{-1}, is ultimately lost from the FT-IR spectrum of the mesoporous films, indicating nearly complete hydrogen bonding of all terminal Si−OH groups with water.

Conclusions

In summary, using real-time FT-IR spectroscopy, we have probed chemical transformations that attend photochemical calcination of surfactants in templated thin film silica mesophases. Grazing incidence difference FT-IR spectroscopy data obtained during the deep-UV exposure process indicate the formation of partially oxidized surfactant intermediates that are ultimately removed from the film at prolonged exposures (>90 min in our illumination geometry). The concentration of these transients appears to peak at a UV exposure time of ∼45 min, when C−H peaks are still present and silicate condensation is incomplete. This suggests that long-chain or cross-linked carboxylated species are formed during the photocalcination process. Changes in the index of refraction of the nanocomposite film were also determined during the deep-UV exposure. The combined FT-IR and index of refraction data collected were both consistent with a stepwise loss of surfactant from the film. The silica condensation was also observed to occur in a process remarkably parallel to the surfactant removal. The concomitant nature of the two processes establishes their cooperativity and provides useful clues for the mechanism by which the mesoscopic order may be transformed (e.g., from the hexagonal mesostructured phase to the cubic mesoporous phase) during the photocalcination process. An additional study is underway to characterize the mesoscopic structural evolution as a function of deep-UV exposure.

Acknowledgment. This work was supported by the Department of Energy Office of Science (Basic Energy Sciences). A.N.P. further acknowledges support from the LANL/UC Davis CARE program.

Supporting Information Available: FT-IR spectra of a mesostructured film exposed to D_2O after 45 min of UV treatment and FT-IR spectra of films exposed to deep-UV light in a reduced oxygen environment, as well as a table of ellipsometric indices of refraction with estimated areas. This material is available free of charge via the Internet at http://pubs.acs.org.

References and Notes

(1) Kresge, C. T.; Leonowicz, M. E.; Roth, W. J.; Vartuli, J. C.; Beck, J. S. *Nature* **1992**, *359*, 710.
(2) Aksay, I. A.; Trau, M.; Manne, S.; Honma, I.; Yao, N.; Zhou, L.; Fenter, P.; Eisenberger, P. M.; Gruner, S. M. *Science* **1996**, *273*, 892.
(3) Yang H.; Kuperman, A.; Coombs, N.; MamicheAfara, S.; Ozin, G. A. *Nature* **1996**, *379*, 703.
(4) Ogawa, M. *Chem. Commun.* **1996**, 1149.
(5) Corma, A. *Chem. Rev.* **1997**, *97*, 2373.
(6) Sayari, A. *Chem. Mater.* **1996**, *8*, 1840.
(7) Stein, A.; Melde, B. J.; Schroden, R. C. *Adv. Mater.* **2000**, *12*, 1403.
(8) Unger, K. K.; Kumar, D.; Grün, M.; Büchel, G.; Lüdtke, S.; Adam, T.; Schumacher, K.; Renker, S. *J. Chromatogr., A* **2000**, *892*, 47.
(9) Feng, X.; Fryxell, G. E.; Wang, L.-Q.; Kim, A. Y.; Liu, J.; Kemner, K. M. *Science* **1997**, *276*, 923.
(10) Schüth, F.; Schmidt, W. *Adv. Mater.* **2002**, *14*, 629.
(11) Scott, B. J.; Wirnsberg, G.; Stucky, G. D. *Chem. Mater.* **2001**, *13*, 3140.
(12) Nguyen, T. Q.; Wu, J.; Doan, V.; Schwartz, B. J.; Tolbert, S. H. *Science* **2000**, *288*, 652.
(13) Sanchez, C.; Lebeau, B.; Chaput, F.; Boilot, J. P. *Adv. Mater.* **2003**, *15*, 1969.
(14) Davis, M. E. *Nature* **2002**, *417*, 813.
(15) Yang, P. D.; Wirnsberger, G.; Huang, H. C.; Cordero, S. R.; McGehee, M. D.; Scott, B.; Deng, T.; Whitesides, G. M.; Chmelka, B. F.; Buratto, S. K.; Stucky, G. D. *Science* **2000**, *287*, 465.
(16) Coakley, K. M.; Liu, Y.; McGhee, M. D.; Frindell, K. L.; Stucky, G. D. *Adv. Funct. Mater.* **2003**, *13*, 301.
(17) Zhou, H. S.; Honma, I. *Adv. Mater.* **1999**, *11*, 683.
(18) Monnier, A.; Schuth, F.; Huo, Q.; Kumar, D.; Margolese, D.; Maxwell, R. S.; Stucky, G. D.; Krishnamurty, M.; Petroff, P.; Firouzi, A.; Janicke, M.; Chmelka, B. F. *Science* **1993**, *261*, 1299.
(19) Beck, J. S.; Vartuli, J. C.; Roth, W. J.; Leonowicz, M. E.; Kresge, C. T.; Schmitt, K. D.; Chu, C. T. W.; Olson, D. H.; Sheppard, E. W.; McCullen, S. B.; Higgins, J. B.; Schlenker, J. L. *J. Am. Chem. Soc.* **1992**, *114*, 10834.
(20) Kleitz, F.; Schmidt, W.; F. Schüth *Microporous Mesoporous Mater.* **2003**, *65*, 1.
(21) Berquier, J.-M.; Nael, P.; Jupille, J.; Jacquiod, C. *J. Sol-Gel Sci. Technol.* **2000**, *19*, 83.
(22) Keene, M. T. J.; Gougeon, R. D. M.; Denoyel, R.; Harris, R. K.; Rouquerol, J.; Llewellyn, P. L. *J. Mater. Chem.* **1999**, *9*, 2843.
(23) Wirnsberger, G.; Scott, B. J.; Stucky, G. D. *Chem. Commun.* **2001**, 119.

(24) Keene, M. T.; Denoyel, R.; Llewellyn, L. *Chem. Commun.* **1998**, 2203.
(25) Hozumi, A.; Sugimura, H.; Hiraku, K.; Kameyama, T.; Takai, O. *Chem. Mater.* **2000**, *12*, 3842.
(26) Clark, T.; Ruiz, J. D.; Fan, H. Y.; Brinker, C. J.; Swanson, B. I.; Parikh, A. N. *Chem. Mater.* **2000**, *12*, 3879.
(27) Vig, J. R. *J. Vac. Sci. Technol., A* **1985**, *3*, 1027.
(28) Dattelbaum, A. M.; Amweg, M. L.; Yee, C.; Ecke, L. E.; Shreve, A. P.; Parikh, A. N. *Nano Lett.* **2003**, *3*, 719.
(29) Lu, Y.; Ganguli, R.; Drewlen, C. A.; Anderson, M. T.; Brinker, C. J.; Gong, W.; Guo, Y.; Soyez, H.; Dunn, B.; Huang, M. H.; Zink, J. I. *Nature* **1997**, *389*, 364−368.
(30) Azzam, R. M. A.; Bashara, N. M. *Ellipsometry and Polarized Light*; Elsevier Science: Amsterdam, The Netherlands, 1987.
(31) Kung, K. H. S.; Hayes, K. F. *Langmuir* **1993**, *9*, 263.
(32) Moller, K.; Bein, T.; Fisher, R. X. *Chem. Mater.* **1995**, *7*, 665.
(33) van Grieken, R.; Calleja, G.; Stucky, G. D.; Melero, J. A.; Garcia, R. A.; Iglesias, J. *Langmuir* **2003**, *19*, 3966.
(34) Geidel, E.; Lechert, H.; Döbler, J.; Jobic, H.; Calzaferri, G.; Bauer, F. *Microporous Mesoporous Mater.* **2003**, *65*, 31.
(35) Bertoluzza, A.; Fagnano, C.; Morelli, M. A. *J. Non-Cryst. Solids* **1982**, *48*, 117.
(36) Innocenzi, P.; Falcaro, P.; Grosso, D.; Babonneau, F. *J. Phys. Chem. B* **2003**, *107*, 4711.
(37) Zhao, X. S.; Lu, G. Q.; Whittaker, A. K.; Millar, G. J.; Zhu, H. Y. *J. Phys. Chem. B* **1997**, *101*, 6525.
(38) Jentys, A.; Kleestorfer, K.; Vinek, H. *Microporous Mesoporous Mater.* **1999**, *27*, 321.
(39) Note that the exact value of the incubation period is a strong function of sample−lamp distance.
(40) Devlin, J. P.; Sadlej, J.; Buch, V. *J. Phys. Chem. A* **2001**, *105*, 974.
(41) Sellinger, A.; Weiss, P. M.; Nguyen, A.; Lu, Y.; Assink, R. A.; Gong, W.; Brinker, C. J. *Nature* **1998**, *394*, 256.
(42) Moon, D. W.; Kurokawa, A.; Ichimura, S.; Lee, H. W.; Jeon, I. C. *J. Vac. Sci. Technol., A* **1999**, *17*, 150.
(43) Brinkmann, M.; Chan, V. Z. H.; Thomas, E. L.; Lee, V. Y.; Miller, R. D.; Hadjichristidis, N.; Avgeropoulos, A. *Chem. Mater.* **2001**, *13*, 967.
(44) Soto-Oviedo, M. A.; Paoli, M. A. D. *Polym. Degrad. Stab.* **2002**, *76*, 219.
(45) Doshi, D. A.; Huesing, N. K.; Lu, M.; Fan, H.; Lu, Y.; Simmons-Potter, K.; Potter, B. G., Jr.; Hurd, A. J.; Brinker, C. J. *Science* **2000**, *290*, 107.
(46) Brunet-Bruneau, A.; Besson, S.; Gacoin, T.; Boilot, J. P.; Rivory, J. *Thin Solid Films* **2004**, *51*, 447.